Catalysis Letters
https://doi.org/10.1007/s10562-020-03326-5

Catalytic Transfer Hydrogenation of Ethyl Levulinate to γ-Valerolactone Over Ni Supported on Equilibrium Fluid-Catalytic-Cracking Catalysts

Han Chen[1] · Qiong Xu[1] · Hui Li[1] · Jian Liu[1] · Xianxiang Liu[1] · Geng Huang[1] · Dulin Yin[1]

Received: 5 March 2020 / Accepted: 20 July 2020

Abstract

Nickel supported on equilibrium fluid-catalytic-cracking catalysts (Ni/E-cats) were prepared by a simple grinding-pyrolysis method and employed for the transfer hydrogenation of ethyl levulinate (EL) to γ-valerolactone (GVL). 96.2% selectivity of GVL and 90.3% conversion of EL were obtained at 180 °C for 6 h over 30-Ni/E-cat. Through XRD, N_2 adsorption–desorption, NH_3-TPD and SEM analysis, the high activity of the 30-Ni/E-cat catalyst was attributed to its dispersed Ni metal active centers and available acidic sites. Catalytic probe test revealed that metal and acid sites of Ni/E-cat played a synergistic catalytic role in the synthesis of GVL in 2-propanol, where Ni metal sites contribute to the hydrogenation of ketone group in EL, and acid sites of E-cat promoted the lactonization of intermediate ethyl- or isopropyl 4-hydroxyvalerate. Two reaction pathways and synergistic mechanism were proposed in this catalytic system. Moreover, Ni/E-cat catalyst exhibited good stability up to four cycles without obvious loss of catalytic activity.

Graphic Abstract

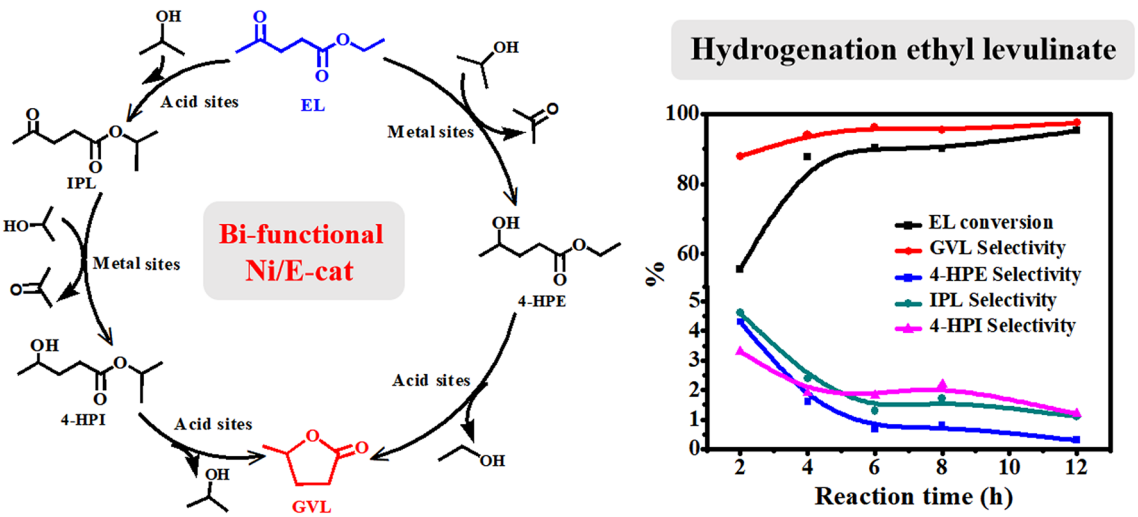

Keywords Ethyl levulinate · γ-Valerolactone · Transfer hydrogenation · Nickel · Equilibrium fluid-catalytic-cracking catalyst

Electronic supplementary material The online version of this article (https://doi.org/10.1007/s10562-020-03326-5) contains supplementary material, which is available to authorized users.

Extended author information available on the last page of the article

Published online: 28 July 2020

1 Introduction

Biomass is the abundant, cheap and renewable organic carbon resource on the earth [1]. The utilization of renewable biomass resources to produce fuels and fine chemicals is of great significance to alleviate the current energy crisis [2, 3]. γ-Valerolactone (GVL), as an important biomass-derived platform molecule, is widely used as fuel additives [4, 5], food additives, green solvents [6, 7] and other valuable chemical intermediates [8, 9].

The hydrogenation-lactonization of biomass-derived levulinic acid (LA) or its esters to GVL is the key reaction in the conversion of biomass to valuable compounds (e.g. gasoline, polyester, etc.). Noble metals, such as Pd [10], Ru [11], Pt [12], exhibited excellent catalytic activities in the production of GVL from LA using H_2 as hydrogen resources. However, the use of noble metal catalysts and high-pressure hydrogen are not preferable from an economical viewpoint. Researchers have turned their attention to non-noble metal catalysts (e.g. Ni [13], Cu [14], Co [15]) and hope to explore an efficient and economical route to synthesize GVL. Among them, Ni catalysts showed a superior activity. Yao Fu's group [13] reported that Raney Ni could efficiently catalyze ethyl levulinate (EL) to synthesize GVL through a catalytic transfer hydrogenation (CTH) process under mild conditions. Unfortunately, the supported Ni catalysts (Ni/C, Ni/TiO_2, Ni/SiO_2, Ni/CeO_2) prepared by them showed poor catalytic activity. Supports with acid sites, such as zeolite, Al_2O_3 or ZrO_2, have been reported to be helpful in the CTH reactions [16–18]. Mohan et al. found that the Ni/H-ZSM-5 catalyst had a high productivity ($0.909 kg_{GVL}.kg_{catalyst}^{-1}\ h^{-1}$) for the hydrogenation of LA to GVL at 250 °C [16]. Cai et al. reported the $10Cu\text{-}5Ni/Al_2O_3$ was an efficient catalyst for the CTH of EL to GVL using 2-butanol as a hydrogen donor, yielding a 97% yield of GVL in 12 h at 150 °C [17]. Sakakibara et al. developed the Ni/ZrO_2 catalyst for the CTH of methyl levulinate to GVL using 2-propanol as a hydrogen donor, and achieved a GVL yield of 94% in 20 h at 100 °C [18]. The excellent performance of the above catalysts was due to the synergistic effect of the metal active center and the acidic carrier. Although these Ni-based catalysts are efficient for the production of GVL from levulinic acid or its esters, the preparation process of the catalysts is complicated and the key step of H_2 reduction can't be avoided, which is not economical for industrial development. Therefore, we plan to use cheap raw materials to prepare an economical and efficient catalyst through a simple method.

Hence, in this work, waste zeolite catalysts generated from the fluid-catalytic-cracking (FCC) process in oil refineries [19, 20], usually called the equilibrium FCC catalyst (E-cat), were used as cheap acid supports to prepare E-cat supported Ni catalysts (Ni/E-cat). The preparation process was simplified into two steps of grinding and pyrolysis, and the self-reduction of metal was achieved during the pyrolysis process under nitrogen. The catalytic performance of the Ni/E-cat catalysts was tested in the CTH of EL to GVL using 2-propanol as a hydrogen donor, and the effects of various parameters including catalyst dosage, reaction temperature, reaction time, different solvents and substrates were also investigated. The two reaction pathways in the reaction and the synergistic catalytic mechanism of the metal and acid sites in this catalytic system were further proposed through the study of reaction process. This work not only provides a new insight for the rational design of highly active Ni-based catalysts for the synthesis of GVL, but also provides an environmentally friendly approach for disposing spent FCC catalysts.

2 Experimental

2.1 Materials

All the reagents used in this study were analytical grade and used as received without further purification. Ethyl levulinate (EL), methyl levulinate (ML), levulinic acid (LA), butyl levulinate (BL), γ-valerolactone (GVL), n-dodecane and 2-butanol (2-BuOH) were purchased from Aladdin Industrial Corporation (Shanghai, China). 2-Propanol (2-PrOH) was purchased from Hunan Huihong Reagent Co., Ltd (Hunan, China). $C_6H_8O_7{\cdot}H_2O$ and $Ni(NO_3)_2{\cdot}6H_2O$ were purchased from Shanghai Wokai Biotechnology Co., Ltd. (Shanghai, China). Equilibrium catalytic cracking catalysts (E-cat) are waste Y-zeolite catalysts produced by the catalytic cracking unit of Sinopec Changling Branch.

2.2 Catalysts Preparation

Ni/E-cat catalysts with different Ni loadings were prepared by a simple grinding-pyrolysis method [21]. A typical catalyst preparing procedure was as follows: $Ni(NO_3)_2{\cdot}6H_2O$ (10 mmol, 2.91 g) and $C_6H_8O_7{\cdot}H_2O$ (5 mmol, 1.05 g) were mixed and ground at room temperature for 0.5 h, then the required amount of E-cat was added and continued grinding for 0.5 h. The mixture changed from solid to homogeneous green paste precursor. The precursor was dried at 120 °C for 4 h in air and calcined for 3 h at 370 °C with ramp rate of 3 °C/min under nitrogen atmosphere. Those prepared catalysts were described as w-Ni/E-cats (where w represents the loading of Ni in wt.%). Ni catalyst was prepared by the same method without adding E-cat. All catalysts were stored in vacuum desiccator and used without further pretreatment.

2.3 Catalyst Characterization

The X-ray fuorescence (XRF) analysis was conducted on a PW2400 spectrometer (Philips, Netherlands) using Rh Kα radiation at 60 kV, 40 mA. Crystal structures of the catalysts were determined by X-ray diffraction (XRD) spectroscopy using an Ultima-IVX-ray powder diffractometer with Cu Kα radiation (λ = 1.5418 Å). Samples were scanned in the 2θ range of 5 ~ 80° at 40 kV and 40 mA with a scan speed of 20°/min. Surface area, pore volume and pore size of the catalysts were obtained from N_2 adsorption–desorption isotherms measured at − 196 °C (TriStar 3000, Micromeritics). Surface area of the catalysts was determined by the BET equation whereas the pore size was measured by the BJH method. Acid amount of catalysts were detected by ammonia temperature-programmed desorption (NH_3-TPD) on a AutoChem II 2920 chemical adsorber (Micromeritics, USA) and the desorbed NH_3 was detected by Thermal Conductivity Detector (TCD). Fourier transforms infrared spectroscopy (FT-IR) analysis was performed on a Perkin Elmer 283 spectrometer, and the FT-IR spectra between 4000 and 400 cm^{-1} were recorded. Thermogravimetric and derivative thermogravimetric (TG-DTG) experiments were obtained on a Netzsch Model STA 409PC instrument. The heating rate from room temperature to 800 °C was 10 °C/min using α-Al_2O_3 as the standard material. The surface morphology and composition of the catalyst were characterized by scanning electron microscopy (SEM, USA, Quanta600F) and X-ray energy spectrometer (EDX, UK, IE350). The operating voltage is 20 kV, the operating current is 5 mA, the working distance is 10 mm, the sample is pasted on the sample table with conductive adhesive, and the surface is sprayed with gold to perform photographing and energy spectrum analysis.

2.4 Catalytic Conversion of EL to GVL

Catalytic conversion of EL to GVL was performed in a 100 mL stainless steel autoclave with Teflon lined reactor under magnetic stirring. In a typical experiment, the reactor was loaded with ethyl levulinate (5 mmol), 2-propanol (19 mL), n-dodecane (1 mmol) and the Ni/E-cat catalyst (216 mg), then purged five times with N_2 at atmospheric conditions before the reaction mixture was heated to the prescribed temperature for a desired reaction time with stirring at 500 rpm. After the reaction, the reactor was cooled to room temperature, and the reaction mixture was magnetically separated from the catalyst. Autoclave containing the separated catalysts was evacuated and refilled with fresh EL solution for subsequent catalytic cycles.

2.5 Sample Analysis

The reaction mixture was analyzed by a gas chromatograph (Shimadzu GC 2014, Japan) with HP-5 column (30.0 m × 0.50 mm × 0.32 μm) and confirmed by a gas chromatograph-mass spectrometer combination (Shimadzu GCMS-QP2010, Japan). The following temperature program was used in the analysis: 55 °C (keeping for 3 min) then increased at a rate of 15 °C/min to 190 °C (held for 1 min). n-Dodecane was used as an internal standard in GC analysis. EL conversion, GVL selectivity and GVL formation rate were calculated using the following equations:

$$EL\ conversion\ (\%) = \left(1 - \frac{Mole\ of\ EL}{Initial\ mole\ of\ EL}\right) \times 100\% \quad (1)$$

$$GVL\ selectivity\ (\%) = \frac{Mole\ of\ GVL}{Initial\ mole\ of\ EL\ -Mole\ of\ EL} \times\ 100\% \quad (2)$$

$$GVL\ formation\ rate\ (mmol/g/h) = \frac{Mole\ of\ GVL}{Amount\ of\ catalyst\ \times\ Reaction\ time} \quad (3)$$

3 Results and Discussion

3.1 Catalyst Characterization

The main chemical composition of E-cat and fresh FCC catalyst (F-cat) was detected by XRF. The results are shown in Table S1. The high silicon and aluminum content is due to the structure of the FCC catalyst itself, containing Y-type zeolite dispersed in a silica-alumina-clay matrix, which is the active component of the FCC catalyst [22]. From the test results, it can be seen that the FCC catalyst used in this work is a Y-type zeolite with lanthanum-cerium rare earth ion exchange. Without unexpectedly, many transition-metal elements (Fe, Ni, V) were also detected in E-cat, which were the elements that caused catalyst poisoning during the catalytic cracking process [23, 24].

The XRD patterns of E-cat and w-Ni/E-cats are shown in Fig. 1. The reflections at 2θ = 5.6 ~ 30.8 and 66.8° were observed in the patterns of all samples, indicating that the Y-zeolite structure of E-cat remained intact after the loading of Ni. All the supported catalysts showed typical XRD reflections at 44.49° (111), 51.85° (200) and 76.38° (220) corresponding to the metallic Ni phase with a face-centered cubic geometry (ICDD. No. 04-002-3695). Moreover, additional diffraction peaks at 37.24° (111), 43.28° (200) and 62.85° (220) were also observed in w-Ni/E-cats,

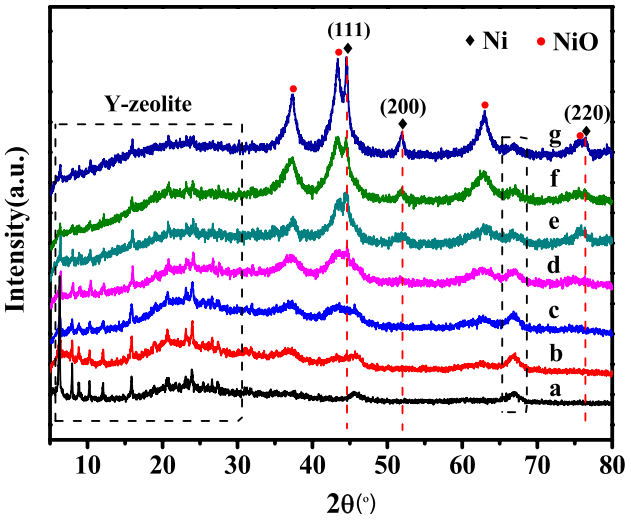

Fig. 1 XRD patterns of the catalysts a E-cat, b 5-Ni/E-cat, c 10-Ni/E-cat, d 20-Ni/E-cat, e 30-Ni/E-cat, f 35-Ni/E-cat and g 40-Ni/E-cat

corresponding to the NiO phase (ICDD. No. 97-002-8834) [25, 26]. The intensity of these peaks increases as the Ni loading of the catalyst increases. The presence of NiO phase in the catalysts suggests that the Ni-citric acid complex precursor wasn't completely reduced during the calcination [27].

Table 1 summarizes the texture properties of F-cat, E-cat and w-Ni/E-cats. The data indicates that all catalysts have mesoporous and microporous structures. It can be clearly seen that the specific area and the pore volume of E-cat are much smaller than those of F-cat. This is because the deposited impurities form some substances destructive to the structure of the molecular sieve at high temperature during the petroleum refining process, resulting in an irreversible change in the structure of the E-cat catalyst [28]. Moreover, the formation of coke covers the surface of the catalyst and blocks the pores of the catalyst [29]. Compared with E-cat, the surface areas and pore parameters of w-Ni/E-cats catalysts decrease with the increase of Ni loading. This implies that nickel metallic particles not only cover the surface of the E-cat carrier, but also are incorporated into the pore channels of the E-cat. The N_2 adsorption isotherms of the catalysts are shown in Fig. S1. The change in the isotherms of the w-Ni/E-cats catalysts is due to the strain of the Ni plugging pore on the zeolite structure [16].

The surface morphologies and compositions of the prepared 30-Ni/E-cat catalyst were examed by SEM measurements (Fig. 2). Micron-sized spherical and irregularly shaped particles were observed. Grooves and cracks were also observed in the sample. The distribution of C, O, Al, Si and Ni elements in the catalyst was probed via SEM mapping. It was found that all these elements C, Ni and O, Al, Si (the composition elements of the molecular sieve) were uniformly dispersed throughout the prepared 30-Ni/E-cat.

The functional groups of E-cat and 30-Ni/E-cat were identified by FT-IR analysis, and the corresponding FT-IR spectra were depicted in Fig. 3. In the FT-IR spectrum of E-cat, the broad peaks at 3440 cm^{-1} and 1625 cm^{-1} are assigned to the -OH bending vibration of physically adsorbed water, and the characteristic absorption peaks in the range of 1380 ~ 490 cm^{-1} belong to the silicon-oxygen tetrahedron, aluminum-oxygen tetrahedron and Si–O–Al structure in the Y-type molecular sieve. Compared with E-cat, a new peak at 456 cm^{-1} appears in the FT-IR spectrum of the 30-Ni/E-cat catalyst, which belongs to the Ni–O bending vibration. This indicates that there is a small amount of NiO in the 30-Ni/E-cat catalyst.

The thermogravimetric analysis results of E-cat and 30-Ni/E-cat are shown in Fig. 4. The slight loss below 200 °C is the removal of physically adsorbed water, indicating that the carrier E-cat is stable. For the 30-Ni/E-cat catalyst, during the entire heating process, the weight loss is divided into three stages, with a weight loss of 6%. Below 200 °C, this corresponds to the loss of absorbed water. A very small weight loss between 200 to 380 °C may be the decomposition of carbon deposits [29]. Combined with the previous characterization, the weight loss of the catalyst at 400 to 500 °C was due to the decomposition of the residual Ni-citric acid precursor during calcination [27]. The low weight loss indicates that there are few undecomposed compounds.

Table 1 Surface areas and pore parameters of the catalysts

Entry	Catalyst	$S_{BET\ surface\ area}$ ($m^2\ g^{-1}$)	$S_{micropore\ surface\ area}$ ($m^2\ g^{-1}$)	$V_{total\ pore\ volume}$ ($cm^3\ g^{-1}$)	$V_{micropore\ pore\ volume}$ ($cm^3\ g^{-1}$)	$D_{average\ pore\ diameter}$ (nm)
1	F-cat	243.1	134.2	0.194	0.0546	12.35
2	E-cat	100.3	54.8	0.152	0.0221	10.84
3	10-Ni/ E-cat	98.2	25.6	0.146	0.0134	7.58
4	20-Ni/ E-cat	97.3	21.3	0.140	0.0106	7.05
5	30-Ni/ E-cat	93.5	17.2	0.138	0.0085	6.84
6	40-Ni/ E-cat	87.9	14.9	0.139	0.0073	6.41

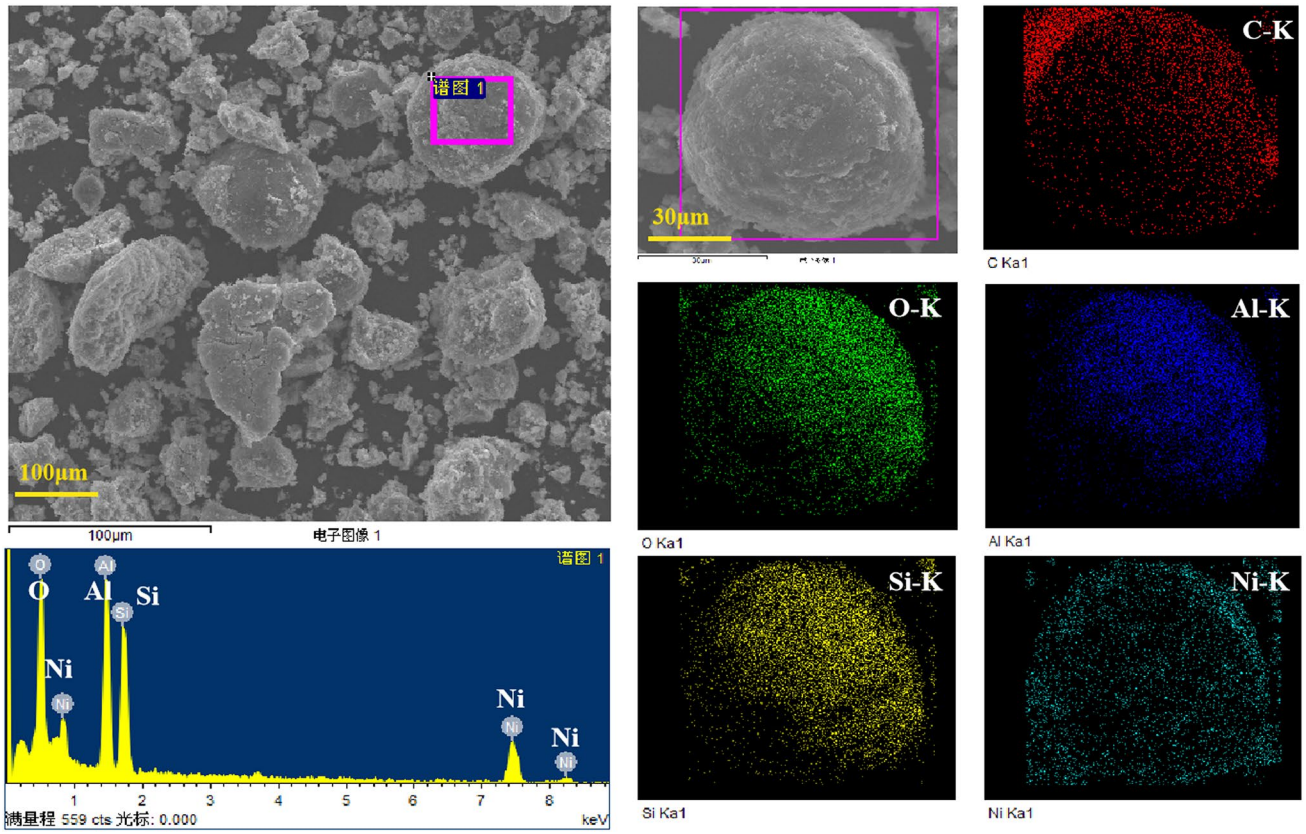

Fig. 2 SEM images with the corresponding elemental mapping (C, O, Al, Si and Ni) and EDX patterns of 30-Ni/E-cat catalyst

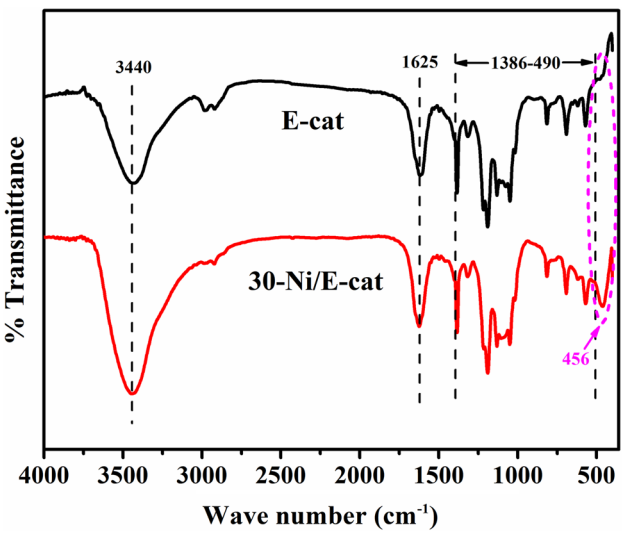

Fig. 3 FT-IR spectra of E-cat and 30-Ni/E-cat

The acid strength distribution and total acidity of E-cat and w-Ni/E-cats were measured by NH_3-TPD, as shown in Fig. S2 and Table S2. The carrier E-cat possesses weak and moderate acid sites. Strong acid sites appear in the spectrum of the w-Ni/E-cat catalysts, and the amount of acid increases with the increase of the Ni loading. Combined with the TG results, a small amount of residual Ni-citric acid complex precursor may be decomposed during the TPD process at 380 ~ 500 °C. Therefore, the data of strong acidity and total acidity of w-Ni/E-cats catalysts are larger. In addition, the presence of a small amount of NiO in w-Ni/E-cats will also lead to an increase in acidity [24]. Among them, the 30-Ni/E-cat catalyst showed a higher concentration of acidic sites (1.242 mmol/g), which could play an important role in the CTH of EL to GVL.

3.2 Catalytic Performance of W-Ni/E-Cat With Different Nickel Loading

The catalytic performance of the w-Ni/E-cat catalysts was evaluated in the CTH of EL to GVL, and the results are listed in Table 2. Only a little transesterified product, isopropyl levulinate (IPL), was detected in the reaction catalyzed by E-cat, showing the acid-catalytic activity of E-cat (Table 2, entry 1). In the w-Ni/E-cat catalyzed reaction, three intermediates ethyl 4-hydroxypentanoate (4-HPE), IPL and isopropyl 4-hydroxyvalerate (4-HPI) as well as the main product GVL were detected. As Ni loading increased in the catalysts,

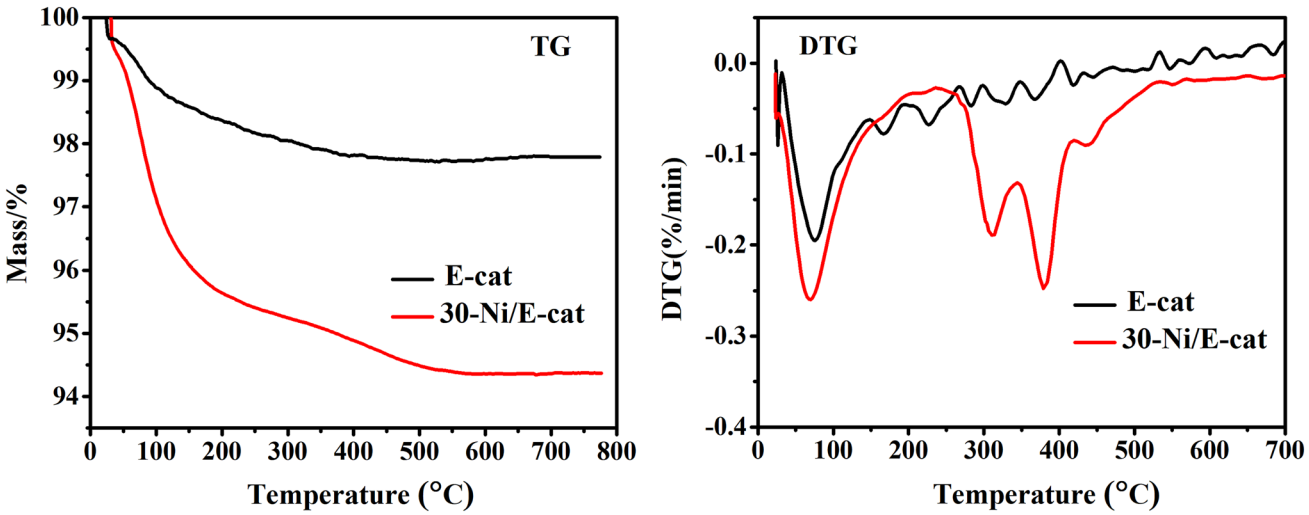

Fig. 4 TG-DTG curves of E-cat and 30-Ni/E-cat

Table 2 Effect of Ni loading on w-Ni/E-cats on the CTH of EL to GVL

Entry	Catalysts	EL conv (%)	Sel. (%)			
			GVL	4-HPE	IPL	4-HPI
1	E-cat	3.2	–	–	100	–
2	5-Ni/E-cat	7.3	43.8	2.8	53.4	–
3	10-Ni/E-cat	9.5	61.1	10.4	27.6	0.9
4	20-Ni/E-cat	18.2	58.1	33.6	7.1	1.2
5	30-Ni/E-cat	52.8	78.3	16.1	4.5	1.1
6	35-Ni/E-cat	25.7	73.8	13.8	11.0	1.4
7	40-Ni/E-cat	8.2	53.9	5.8	38.4	1.9

Reaction conditions: 5 mmol EL, 19 mL 2-propanol, 50 mg catalyst, 1 mmol n-dodecane, 180 °C, 4 h

EL conversion and GVL selectivity gradually increased, while the selectivity of IPL reduced rapidly. The selectivity of the intermediate ethyl 4-hydroxypentanoate (4-HPE) and isopropyl 4-hydroxypentanoate (4-HPI) increased slightly (Table 2, entries 2–4). This implies that there are two different pathways in the reaction catalyzed by metal–acid bi-functional catalysts. More details about the pathway are further discussed in Section 3.6. The 30-Ni/E-cat catalyst showed superior catalytic performance in the hydrogenation reaction, providing an EL conversion of 52.8% and a GVL selectivity of 78.3% (Table 2, entry 5). However, an excessive loading of Ni led to a decrease in EL conversion and GVL selectivity (Table 2, entries 6–7). This was because feeding more nickel nitrate during the preparation process might cause the agglomeration of Ni particles and reduce the dispersion of Ni active centers, thereby reducing the activity of the catalyst. These results indicate that the combination of Ni and E-cat is a promising catalyst with an optimal Ni loading of 30%.

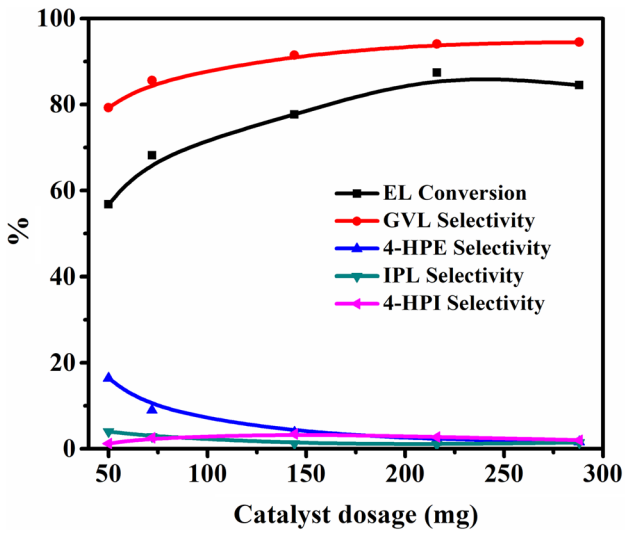

Fig. 5 Effect of catalyst dosage on the CTH of EL to GVL. Reaction conditions: 5 mmol EL, 19 mL 2-propanol, 30-Ni/E-cat, 1 mmol n-dodecane, 180 °C, and 4 h

3.3 Effect of Catalyst Dosage

The effect of catalyst dosage on the CTH of EL to GVL was studied and results are presented in Fig. 5. Those experiments were carried out by changing the dosage of 30-Ni/E-cat from 50 to 288 mg while keeping the reaction temperature at 180 °C and the reaction time for 4 h. Obviously, both EL conversion and GVL selectivity were increased and the selectivity of the intermediate product 4-HPE gradually decreased with increasing the catalyst dosage, which should be mainly attributed to more available number of catalytically active sites. In the presence of large amount of metal catalytic sites, the transesterified product IPL and intermediate 4-HPI were very little. When the catalyst dosage was 216 mg, a GVL selectivity of 94.1% was obtained at an EL conversion of 87.7%. However, a further increase of catalyst dosage (288 mg) led to the EL conversion slightly decreased to 84.5% although the selectivity of GVL was still increased, which possibly attributed to excessive metal catalysts hindering contact with the substrate. Therefore, 216 mg was selected as the optimal catalyst dosage for the subsequent experiments.

3.4 Effect of Reaction Temperature and Time

The reaction temperature has an important effect on the reaction rate and products distribution. Thus, the CTH of EL was carried out at different reaction temperatures, ranging from 160 to 190 °C (Fig. 6a). When the reaction proceeded at a milder condition (160 °C), 55.3% conversion of EL and 66.8% selectivity of GVL were achieved. With the increase of the reaction temperature, the EL conversion and GVL selectivity continuously increased until a maximum GVL selectivity of 94.1% was obtained at 180 °C. This was possibly attributed to the increase of the reaction rate at higher reaction temperature. Further increasing the reaction temperature to 190 °C led to a slight decrease of GVL selectivity. It was likely that the product might undergo some side reactions at higher reaction temperature. Meanwhile, the reaction was also traced to investigate the influence of the reaction time on the CTH reaction (Fig. 6b). It is worth noting that when reaction time from 2 h was prolonged to 12 h, the conversion of EL increased greatly from 55.8% to 95.2%, but the selectivity of GVL changed little (91.1% to 97.4%). Correspondingly, the selectivity of the three intermediate products was less than 5%, and gradually decreased with the extension of time. This indicates that enough acid sites on the carrier promote the rapid conversion of intermediate products to GVL, and the hydrogenation of EL is the rate-limiting step in the reaction. The conversion of EL was increased by only 4.9% when the time increased from 6 to 12 h. Those observations suggest that the reaction time beyond 6 h hardly affects the EL conversion. Based on the above experiments, the optimal reaction temperature of 180 °C and reaction time of 6 h were sufficient for the CTH reaction of EL to achieve high GVL yield.

3.5 Effect of Different Alcohols and Substrates

In the CTH reaction, alcohols are not only the solvent but H-donors. 1-propanol (1-PrOH), 2-propanol (2-PrOH), 2-butanol (2-BuOH) and cyclohexanol (CyOH) were chosen as the solvent and H-donors in this reaction. As shown in Table 3, secondary alcohols provided high EL

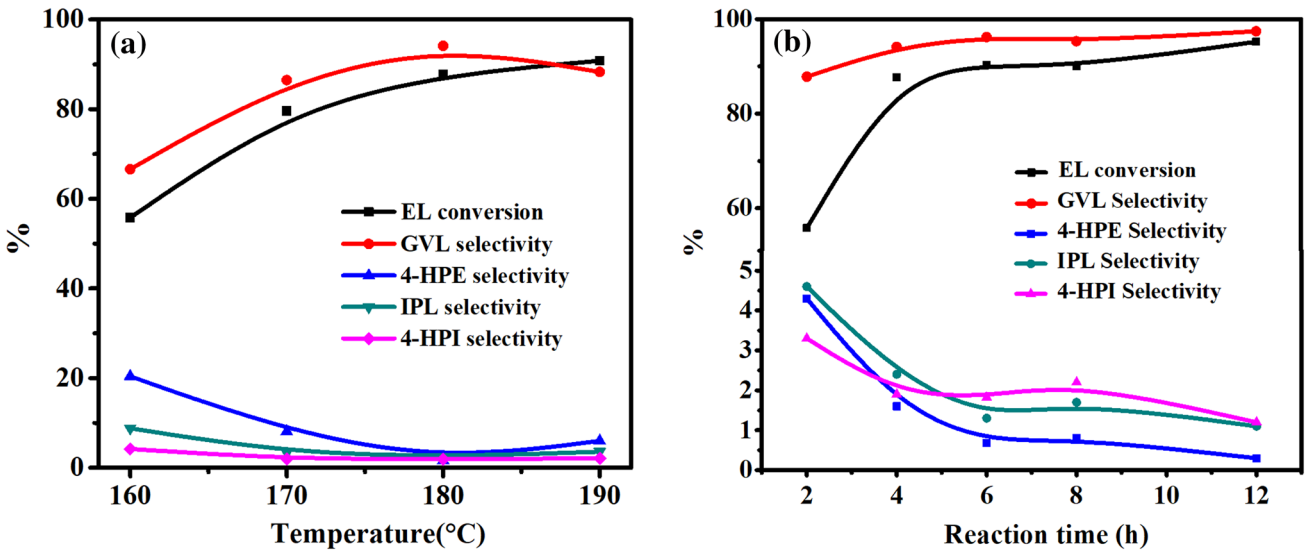

Fig. 6 Effect of reaction temperature (**a**) and reaction time (**b**) on the CTH of EL to GVL. Reaction conditions: 5 mmol EL, 19 mL 2-propanol, 216 mg 30-Ni/E-cat, 1 mmol n-dodecane, **a** 4 h; **b** 180 °C

Table 3 Catalytic feasibility of 30-Ni/E-cat in different alcohols and substrates

Entry	Substrate	Solvent	Conversion (%)	GVL selectivity (%)	GVL formation rate (mmol/g/h)
1	EL	1-PrOH	65.8	11.9	0.30
2	EL	2-PrOH	90.3	96.2	3.35
3	EL	2-BuOH	76.6	90.1	2.66
4	EL	CyOH	30.3	12.6	0.15
5	ML	2-PrOH	86.7	92.5	3.09
6	BL	2-PrOH	95.9	95.6	3.54
7	LA	2-PrOH	90.2	91.4	3.18

Reaction conditions: 5 mmol EL, 19 mL solvent, 216 mg 30-Ni/E-cat, 1 mmol n-dodecane, 180 °C, 6 h

conversion, GVL selectivity and GVL formation rate, as opposed to primary alcohols. The hydrogen-donating ability of alcohols decreased in the order of: 2-PrOH>2-BuOH>1-PrOH>CyOH, which was consistent with many previous reported works [13, 17, 30]. According to the literature report, the primary alcohols were poor H-donors in the CTH reaction due to the difficult β-hydride elimination after it formed alkoxy species on the surface of the catalyst [17]. CyOH was not an effective H-donor in this reaction, which might due to the strong steric hindrance effect of the solvent. Considering reactivity and practicality, 2-PrOH was the best choice as a solvent and hydrogen source in our reaction system.

In addition, other levulinate esters including Methyl levulinate (ML), butyl levulinate (BL) and levulinic acid (LA) were also applied to the CTH reaction for the production of GVL. High conversion and GVL selectivity were obtained in the reactions catalyzed by the 30-Ni/E-cat catalyst, which indicates that the bi-functional catalyst has a promising potential for converting biomass derivatives into GVL.

3.6 The Catalytic Roles of Ni and E-cat in Ni/E-cat Catalyst

To explore the role of Ni and E-cat in the CTH reaction, Ni, physically mixed Ni and E-cat, fresh and poisoned 30-Ni/E-cat (adding pyridine or thiol) were used in the reaction to compare their catalytic activities. Results are given in Table 4. Comparing the results of entries 1–3, monometallic Ni showed poor catalytic performance, providing only 7.8% conversion of EL and 39.9% selectivity of GVL. However, the selectivity of the intermediate 4-HPE was high, reaching 60.1% (Table 4, entry 1). It was interesting that once the co-operation of nickel with acidic E-cat, whether a physically mixed Ni + E-cat (Table 4, entry 2) or a co-pyrolysis Ni/E-cat (Table 4, entry 3), both exhibited enhanced catalytic performance in the reaction. The selectivity of GVL on Ni/E-cat or Ni + E-cat was substantially higher than that on sole Ni, which may benefit from the inner transesterification of the intermediate 4-HPE promoted by the surface acidic sites of E-cat [18, 28]. When the poison probe thiol was introduced into the reaction system, EL conversion and GVL formation rate decreased sharply, but the selectivity of the acid-catalytic product IPL was improved (Table 4, entry 4). This is because the Ni metal sites of Ni/E-cat are poisoned, weakening the hydrogenation function of the catalyst. Besides, no 4-HPI was detected in this reaction, indicating that the formation of 4-HPI is not an acid-catalyzed reaction but a hydrogenation reaction. The little 4-HPI (in Table 4, entries 2, 3 and 5) can be the hydrogenation product of IPL catalyzed by Ni sites. Adding pyridine as an alkaline probe molecule to the reaction, the acidic sites on Ni/E-cat were almost poisoned,

Table 4 Catalytic activities of different catalysts with metal and (or) acid sites[a]

Entry	Catalyst	EL conv (%)	Sel. (%)				GVL Formation rate (mmol/g/h)
			GVL	4-HPE	IPL	4-HPI	
1[b]	Ni	7.8	39.9	60.1	–	–	2.59
2[c]	Ni + E-cat	48.9	81.6	13.1	3.4	1.9	9.98
3	30-Ni/E-cat	52.8	78.3	16.1	4.5	1.1	10.32
4[d]	thiol-30-Ni/E-cat	6.3	68.9	14.3	16.8	–	1.09
5[e]	pyridine-30-Ni/E-cat	43.7	42.2	54.3	1.3	2.2	4.61

Reaction conditions:

[a]5 mmol EL, 19 mL 2-propanol, 1mmoln-dodecane, 50 mg catalyst, 180 °C, 4 h

[b]Ni was 15 mg

[c]Ni + E-cat: physical-mixed Ni and E-cat (Ni was 15 mg and E-cat was 35 mg)

[d]Adding thiol to the reaction system

[e]Adding pyridine to the reaction system

resulting in lower GVL selectivity and higher 4-HPE selectivity, which was close to the process of using monometallic Ni (Table 4, entry 5). From the above experimental results, it can be concluded that metallic Ni contributes to the transfer hydrogenation of EL/IPL with 2-propanol, and acidic E-cat promotes the lactonization of the hydrogenated product 4-HPE/4-HPI to GVL.

3.7 Propose Reaction Pathways and Synergistic Mechanism

Based on the above results, we draw up two pathways for the conversion of EL to GVL using 2-propanol as a hydrogen donor over Ni/E-cat catalysts (shown in Scheme 1). The one is that EL was firstly hydrogenated to form the intermediate 4-HPE on the Ni sites, and subsequent 4-HPE was cyclized by inner transesterification on acid sites to generate GVL. This is the major route in the CTH of EL to GVL catalyzed by Ni/E-cat. The other is that EL firstly underwent transesterification with 2-propanol on the acid sites to form IPL, and IPL was hydrogenated to form the intermediate 4-HPI, which was then further converted to GVL on the acid sites.

The synergistic mechanism based on the 4-HPE-mediated major pathway is deduced. Firstly, 2-propanol and EL are adsorbed on the metal sites (Ni) and acid sites on the surface of the catalyst, respectively. The adsorption of 2-propanol breaks the C–H and O–H bonds to release acetone, thus two H-atoms remained on the Ni surface, which is the active species for transfer hydrogenation. These two H-atoms are transferred to the ketone group of EL existing on the adjacent surface site of the catalyst, and the EL undergoes a hydrogenation reaction to form the intermediate 4-HPE. Finally, the hydrogenated product 4-HPE is easily cyclized on the acidic sites to produce the GVL.

3.8 Reuse Test

The recyclability of 30-Ni/E-cat was investigated in the CTH of EL to GVL under the optimal reaction condition. After each run, the catalyst was separated from the reaction mixture by a magnet, washed with 2-propanol three times, and then directly subjected to the next run without adding any fresh catalyst. The results are presented in Fig. 7. The catalyst was used for four catalytic runs with only a slight decrease in the EL conversion, and the GVL selectivity kept well in the reaction.

To figure out the change of the catalyst during the reaction, XRD and SEM were further carried out to characterize the spent catalyst. Fig. S3 showed the XRD analysis of the fresh and spent 30-Ni/E-cat catalyst. The two patterns showed similar diffraction peaks, which indicated that the active metal sites on the surface of the 30-Ni/E-cat catalyst were almost unchanged after being recycled four consecutive times. Fig. S4 showed some representative SEM images of the fresh and spent 30-Ni/E-cat catalyst. Compared with the fresh 30-Ni/E-cat (Fig. S4a, b), the metal particles could still be well dispersed after the reaction. However, the surface of the used 30-Ni/E-cat became smooth (Fig. S4c, d). This might be caused by the wear between the magneton and the catalyst during the thermal solution reaction, which might be unavoidable for most supported FCC catalyst under such reaction condition. However, the reactivity of the catalyst remained at a

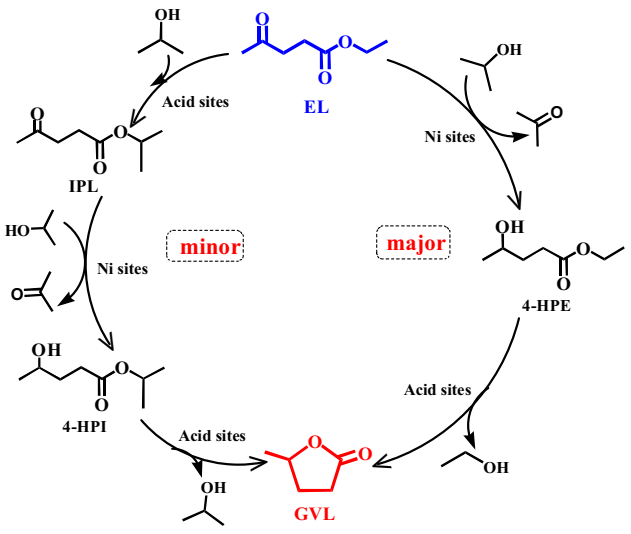

Scheme 1. The reaction mechanism for conversion of EL to GVL over bi-functional Ni/E-cat catalyst

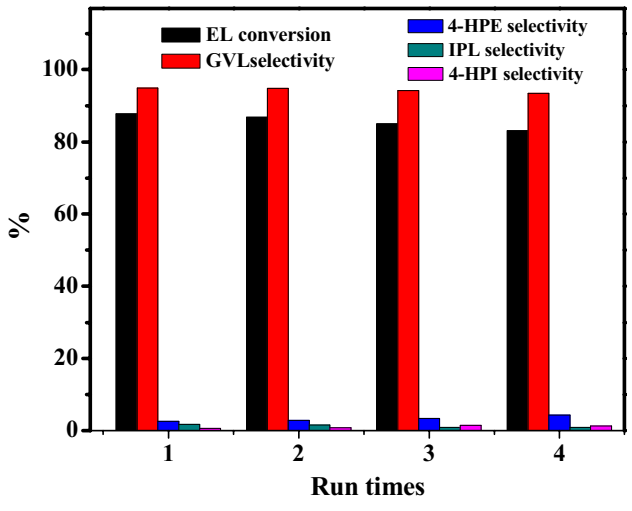

Fig. 7 Reuse of 30-Ni/E-cat in the CTH of EL to GVL. Reaction conditions: 5 mmol EL, 19 mL 2-propanol, catalyst dosage 216 mg, 1 mmol n-dodecane, 180 °C, 4 h

relatively high level despite some surface wear. This result further confirms that the 30-Ni/E-cat catalyst has a good stability under the CTH reaction conditions.

4 Conclusions

In this work, we reported a robust and efficient metal–acid bi-functional 30-Ni/E-cat catalyst for the transfer hydrogenation of ethyl levulinate to γ-valerolactone. An excellent catalytic performance with 96.2% GVL selectivity and 90.3% EL conversion was obtained in the CTH reaction using 2-PrOH as a H-donor at 180 °C for 6 h. Both Ni and the carrier E-cat contributed significantly to the excellent performance of Ni/E-cat. Metallic nickel sites in the 30-Ni/E-cat largely contributed to the hydrogenation of EL, and acid sites of E-cat played a synergistic catalytic role by promoting the cyclization of the intermediate 4-HPE. This is the dominant pathway mediated by the intermediate 4-HPE. Besides, GVL was also produced by another pathway of the intermediates IPL/4-HPI. We believe that the highly efficient and easily prepared Ni/E-cat catalysts have great potential of application in hydrogenation reactions, and the waste E-cat can also be reused to prepare other effective supported bi-functional catalysts.

Acknowledgements The authors gratefully acknowledge the financial support of the National Natural Science Foundation of China (Grant No. 21776068, 21606082 and 21975070) and Scientific Research Fund of Hunan Provincial Education Department (17C0951 and 15B050).

Compliance with Ethical Standards

Conflict of interest The authors declare that they have no conflicts of interest.

References

1. Corma A, Iborra S, Velty A (2007) Chem Rev 107:2411–2502
2. Li C, Zhao X, Wang A, Huber GW, Zhang T (2015) Chem Rev 115:11559–11624
3. Kunkes EL, Simonetti DA, West RM, Juan Carlos SR, Gärtner CA, Dumesic JA (2008) Science 322:417–421
4. Horváth IT, Mehdi H, Fábos V, Boda L, Mika LT (2008) Green Chem 10:238–242
5. Bruno TJ, Wolk A, Naydich A (2010) Energy Fuels 24:2758–2767
6. Wettstein SG, Alonso DM, Chong Y, Dumesic JA (2012) Energy Environ Sci 5:8199
7. Mellmer MA, Martin Alonso D, Luterbacher JS, Gallo JMR, Dumesic JA (2014) Green Chem 16:4659–4662
8. Du X-L, Bi Q-Y, Liu Y-M, Cao Y, He H-Y, Fan K-N (2012) Green Chem 14:935–939
9. Al-Shaal MG, Dzierbinski A, Palkovits R (2014) Green Chem 16:1358–1364
10. Zhang Y, Chen C, Gong W, Song J, Zhang H, Zhang Y, Wang G, Zhao H (2017) Catal Commun 93:10–14
11. Sudhakar M, Lakshmi Kantam M, Swarna Jaya V, Kishore R, Ramanujachary KV, Venugopal A (2014) Catal Commun 50:101–104
12. Upare PP, Lee J-M, Hwang DW, Halligudi SB, Hwang YK, Chang J-S (2011) J Ind Eng Chem 17:287–292
13. Yang Z, Huang YB, Guo QX, Fu Y (2013) Chem Commun (Camb) 49:5328–5330
14. Yang Y, Xu X, Zou W, Yue H, Tian G, Feng S (2016) Catal Commun 76:50–53
15. Zhou H, Song J, Fan H, Zhang B, Yang Y, Hu J, Zhu Q, Han B (2014) Green Chem 16:3870–3875
16. Mohan V, Raghavendra C, Pramod CV, Raju BD, Rama Rao KS (2014) RSC Adv 4:9660
17. Cai B, Zhou X-C, Miao Y-C, Luo J-Y, Pan H, Huang Y-B (2016) ACS Sustain Chem Eng 5:1322–1331
18. Sakakibara K, Endo K, Osawa T (2019) Catal Commun 125:52–55
19. Bertero M, García JR, Falco M, Sedran U (2019) Renew Energy 132:11–18
20. Zhang D, Wen B, Chen Y, Xu Q, Zhu X, Sun N, Liu X, Yin D (2020) J Mater Cycles Waste Manag 22:22–29
21. Venkatesha NJ, Ramesh S (2018) Ind Eng Chem Res 57:1506–1515
22. Liu H, Ma J, Gao X (2006) Catal Lett 110:229–234
23. Souza NLA, Tkach I, Morgado E, Krambrock K (2018) Appl Catal A 560:206–214
24. Gerards RTJ, Fernandes A, Graça I, Ribeiro MF (2020) Fuel 260:116372
25. Kumar VV, Naresh G, Sudhakar M, Anjaneyulu C, Bhargava SK, Tardio J, Reddy VK, Padmasri AH, Venugopal A (2016) RSC Adv 6:9872–9879
26. Singh H, Iyengar N, Yadav R, Rai A, Sinha AK (2018) Sustain Energy Fuels 2:1699–1706
27. Abu-Zied BM, Asiri AM (2017) Thermochim Acta 649:54–62
28. Cho SI, Jung KS, Woo SI (2001) Appl Catal B 33:249–261
29. Su B, Shi L, Meng X, Wang X, Liu N (2018) J Sulfur Chem 40:75–87
30. He J, Li H, Lu Y-M, Liu Y-X, Wu Z-B, Hu D-Y, Yang S (2016) Appl Catal A 510:11–19

Affiliations

Han Chen[1] · Qiong Xu[1] · Hui Li[1] · Jian Liu[1] · Xianxiang Liu[1] · Geng Huang[1] · Dulin Yin[1]

✉ Qiong Xu
xuqiong@hunnu.edu.cn

✉ Dulin Yin
dulinyin@126.com

[1] National and Local Joint Engineering Laboratory for New Petro-Chemical Materials and Fine Utilization of Resources, College of Chemistry and Chemical Engineering, Hunan Normal University, Changsha 410081, China